

Formulation of a Surf-Similarity Parameter to Predict Tsunami Characteristics at the Coast

Jochem J. Roubos¹, Toni Glasbergen², Bas Hofland³, Jeremy D. Bricker⁴, Marcel Zijlema⁵, Miguel Esteban⁶, and Marion F. S. Tissier⁷

Abstract

To calculate tsunami forces on coastal structures it is of great importance to determine the shape of the tsunami front reaching the coast. Based on literature reviews, analytical reasoning, video footage, and numerical modelling it is concluded that both the continental shelf slope and the bay geometry have a significant influence on the transformation of a tsunami wave near the coastline. After conducting 1D and 2DH wave simulations, a distinction is made between three types of tsunami waves; a non-breaking front (surging), a breaking front and an undular bore breaking front. Tsunami waves transform into these three wave types over a steep continental shelf, an intermediate sloped continental shelf, and a gentle sloped continental shelf, respectively. A new tsunami surf-similarity parameter is proposed to quantitatively predict the type of wave at the coastline, which was validated based on observations during the *2011 Tohoku Earthquake and Tsunami*.

Keywords

Tsunami, Surf-similarity Parameter, Undular Bore, Wave Front Breaking, Surging, Continental Shelf, Bay Geometry

1 Introduction


The *2011 Tohoku Earthquake and Tsunami* was one of the most devastating such events to affect the Japanese coastline (Mori et al., 2012; Wei et al. 2012). Prior to the 2011 event the coastlines of this region had been protected by seawalls and sea dykes, some higher than 10 m, though the tsunami overtopped and destroyed many of them (Jayaratne et al., 2016). A large variation in tsunami inundation and run-up heights was observed along the east coast of Japan (Mikami et al., 2012), and its behaviour showed a clear

¹jochemroubos@gmail.com, Van den Herik, Sliedrecht, The Netherlands
²toniglasbergen92@gmail.com, Jelmer, Vinkeveen, The Netherlands
³B.Hofland@tudelft.nl, Delft University of Technology, Delft, The Netherlands
⁴jeremydb@umich.edu, University of Michigan, Michigan, United States
⁵M.Zijlema@tudelft.nl, Delft University of Technology, Delft, The Netherlands
⁶esteban.fagan@gmail.com, Waseda University, Tokyo, Japan
⁷M.F.S.Tissier@tudelft.nl, Delft University of Technology, Delft, The Netherlands

This paper was submitted on 9 March 2020. It was accepted after double-blind review on 2 November 2021 and published online on 17 December 2021.

DOI: <https://doi.org/10.48438/jchs.2021.0009>

Cite as: "Roubos, J., Glasbergen, T., Hofland, B. ., Bricker, J., Zijlema, M., Esteban, M., & Tissier, M. Formulation of a Surf-Similarity Parameter to Predict Tsunami Characteristics at the Coast. Journal of Coastal and Hydraulic Structures, 1, p. 9. <https://doi.org/10.48438/jchs.2021.0009>"

The Journal of Coastal and Hydraulic Structures is a community-based, free, and open access journal for the dissemination of high-quality knowledge on the engineering science of coastal and hydraulic structures. This paper has been written and reviewed with care. However, the authors and the journal do not accept any liability which might arise from use of its contents. Copyright ©2020 by the authors. This journal paper is published under a CC-BY-4.0 license, which allows anyone to redistribute, mix and adapt, as long as credit is given to the authors. 

regional dependence due to variations in bathymetry and topography (as the Tohoku coastline consists of two distinctive geographical zones, namely the Sendai Plain and the Sanriku coastline). While the Sendai Plain features a fluvial lowland and a flat coastal plain, the Sanriku coast is known as a ‘ria-coast’, where coastal inlets were formed through the inundation by the sea of former river valleys. The resulting coastline is heavily indented, consisting of numerous small bays of variable geometry, similar to fjords, as shown in Figure 1.

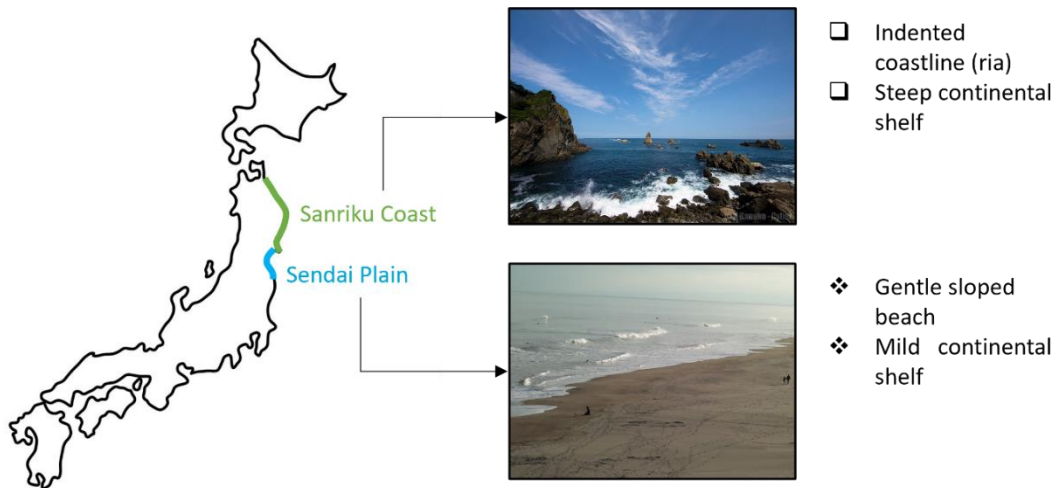


Figure 1: Characteristics of the Tohoku coastline: Sanriku coast (Reprinted from *Flickr*, by Author H. Kaneko, 2014, Retrieved from <https://www.flickr.com/photos/cyber0515/15428369395/>) and Sendai Plain (Retrieved from *Flickr*, by Author K. Chiba, 2010, Retrieved from <https://www.flickr.com/photos/118377396@N08/25623488718/>).

Observed tsunamis hitting a coastline have been classified into three categories; (1) rapidly rising tide, (2) breaking bore or wall of water, and (3) undular bore (Sriram et al. 2016, Shuto 1985, Larsen and Fuhrman 2019). Shimonzono et al. (2012) studied the behaviour of the 2011 tsunami wave along the central Sanriku coast, and observed variations depending on the section of coastline. The waves exhibited breaking progressive wave crests over gentle slopes, while they had the features of surging waves over steep slopes. During recent major tsunami events (2004 *Indian Ocean Tsunami* and 2011 *Tohoku Earthquake and Tsunami*), the observed waves were sometimes described as a series of relatively short (typically 10-15 s) breaking waves in front of the coastline. However, it is most likely that these were resulting from the breaking of the short wave train that develops behind the leading tsunami front when undular bores form (e.g., Grue et al., 2008; Madsen et al., 2008; Tissier et al., 2011).

Madsen et al. (2008) investigated the transformation of tsunami-like waves into undular bores and their subsequent splitting into a series of solitons. They showed that a full splitting of the initial tsunami wave into solitons was unlikely to happen due to geophysical constraints, and thus concluded that tsunami run-up was mostly driven by the underlying long wave rather than by the undulations. More recently, Larsen and Fuhrman (2019) applied a detailed numerical model with a Volume of Fluid free surface treatment to study the breaking and runup of tsunamis (modelled by solitons and N-waves) in two-dimensional cases. It was observed that undular bores appear during propagation over mildly sloping coasts. The undulations could maintain their shape up to the shore, or break far offshore creating a breaking bore. However, the limiting value of a parameter predicting the type of breaking behaviour was not given. Larsen & Fuhrman (2019) finally confirmed that the development of the short waves had little impact on the tsunami run-up and inundation speed, but highlighted their importance in terms of local flow velocities.

The formation of (stationary) undular bores on flat beds has been studied by many researchers. Benjamin and Lighthill (1954) showed that, for bores of moderate Froude numbers, the energy that should be lost according to conservation laws radiates away from the front through the generation of short waves, instead of being dissipated through breaking. Binnie and Orkney (1955) report the formation of undular and regular breaking bores in experiments in a horizontal channel, and showed that undular bores develop for Froude numbers below 1.26. Peregrine (1966) calculated that the bore will be undular if the change in surface elevation of the wave is less than 0.28 of the original depth of water. Tsuji et al. (1991) report about the wave shape of tsunamis advancing in rivers, and show that both undular and breaking bores are solutions of the KdV-Burger's equation for shallow water flows. For small depth differences between incoming wave and original water depth undular bores occur with a maximum crest height of about 1.5 times the height of the initial bore.

Bore formation influences the wave speed and thus for the potential impulsive impact of the tsunami front on a seawall. ASCE (2016) assumes that the Froude number at the coastline, which is related to the flow velocity at the coastline, is 1.0 for situations without bore formation and 1.3 for situations with bore formation, which results in a bigger impact on the structure for tsunamis with bore formation than for those without bore formation.

The most important wave forces on a seawall or dyke are the hydrostatic force F_h , the hydrodynamic forces F_d and impulsive forces F_s , according to FEMA (2012). Impulsive forces are important for the design of a seawall or sea dyke, since the force during the initial impact can be approximately 50% higher than the hydrodynamic force during the bore passing, according to the experiments of Árnason (2015). The hydrodynamic force is related to the maximum momentum flux, which is an important parameter in the present study.

The Iribarren number ζ (see Battjes, 1974), eq. (1), gives an expression for the relationship between non-breaking and breaking progressive waves on a slope. This parameter expresses the type of breaking - a spilling wave, a plunging wave or a surging wave - which will occur for certain wave characteristics and a given bathymetric slope.

$$\zeta = \frac{\tan(\alpha)}{\sqrt{H/L_o}} \tag{ 1 }$$

where α is the seaward slope of the structure, H is the wave height and L_o is the deep-water wavelength.

Surf-similarity parameters such as the Iribarren number are often used for analyzing tsunami run-up (Madsen & Fuhrman, 2019; ASCE, 2016). However, this surf-similarity parameter cannot be used in the case where wave focusing is expected (ASCE, 2016), such as in the bays along the Sanriku coast. It is well known that the run-up and wave shoaling of tsunamis can be intensified when they approach U-shaped bays (Didenkulova and Pelinovsky, 2011). According to Bonneton et al. (2015) the theory behind tsunami wave transformation in bays along the Sanriku coast can be used as a starting point regarding the formation and dynamics of tidal bores in funnel-shaped estuaries. These authors showed that tidal bore formation is mainly governed by a dissipative parameter D , which characterizes the amount of nonlinearity. When D is large, the dissipative character of the estuary is large, and the conditions are favorable for bore formation. Dissipation is enhanced by increasing tidal range, friction coefficient and convergence length, and decreasing water depth. To see if these parameters are also important for tsunami wave transformation in a bay, the influence of tsunami wave characteristics (wave height and wavelength) and bay geometry will also be investigated in the present study.

Figure 2 provides several snapshots of video footage taken along the Tohoku coastline during the 2011 tsunami, showing how the wave front can be broken (breaking wave front or series of bores) or non-broken (surging/rising water level). Along the Sanriku coastline, where the slope of the continental shelf is rather steep, different types of tsunami waves were observed. The left part of Figure 2 shows the broken wave front that was observed at Kuji Bay, and the middle part of Figure 2 a non-broken surging wave that propagated into Miyako Bay. Near the Sendai Plain a series of tsunami bores developed in front of the coastline (right part of Figure 2). Prior to the 2011 Tohoku Earthquake and Tsunami research had focused on the difference between wet-bed bores and dry-bed surges (e.g. Ramsden, 1993; Yeh, 2006; St. Germain and Nistor, 2012; Koch and Chanson, 2009). However, such discussions cannot accurately explain the phenomenon shown by Fig 3b, in which a long wave reflects from a steep coastline without bore formation. Essentially, this phenomenon is more similar to a surging breaker, as defined for sea and swell waves (Battjes, 1974), and the authors will hereafter refer to this as a surge-type tsunami, following Bricker and Nakayama (2014).



Figure 2: Observation of different tsunami wave types at several locations along the Tohoku coastline during the 2011 Tohoku Earthquake Tsunami. Left to right: Kuji Bay (Topics, 2016), Miyako Bay (Topics, 2017), Sendai coast (Topics, 2018).

Following the 2011 tsunami event, the Japanese government changed the design policy regarding countermeasures (Shibayama et al., 2013), which has resulted in the construction of higher seawalls and sea dykes. However, given the variety of waveforms that can take place (as shown in Figure 2), uncertainties in wave type and resulting loading complicates the design of coastal structures. Essentially, a more quantitative understanding of tsunami wave transformation is needed to predict the impact that such waves can have on coastal defense systems along the Tohoku coastline and to increase the safety of these systems in the future. The aim of the present research is to achieve this based on literature reviews, analytical reasoning, video footage, and numerical modelling.

The differences in wave types along the Tohoku coastline will be investigated, where the steep ria coast of Sanriku will be compared to the gentle sloped Sendai Plain (Figure 1). Using simple analytical reasoning a new surf-similarity parameter is introduced in section 2.1. Then, the geometrical characteristics of various locations along the Japanese coast is determined, and based on video footage the type of tsunami wave breaking in 2011 is determined in section 2.2. As a next step, a numerical model is set up and validated for wave breaking in section 3 to simulate the breaker type for this range of parameters. Finally, the prediction of the breaker type by the newly proposed surf-similarity parameter is validated for the tsunami breaker types observed in 2011.

The main focus of this research is the type of tsunami wave front (occurrence of bore), since the impact on the coastal structure differs for a broken or a non-broken tsunami wave. The parameter range considered is based on the coastal shapes that are present along the Tohoku coastline. The difference between plunging and spilling waves is not considered, as the model used to calculate the tsunami propagation has a single free surface, so it cannot resolve this difference.

2 Methods

2.1 Tsunami surf-similarity parameter

As noted by ASCE (2016), it is important to know if the front of a tsunami wave breaks, due to the different effect that this can have on coastal structures and other infrastructure. To improve the classification of tsunami waves approaching the shore for 1D situations, a tailored surf-similarity parameter $\xi_{tsunami,1D}$ for tsunamis, based on the Iribarren number ζ , was proposed by Glasbergen (2017) as shown by eq. (2). To investigate what parameters define this wave breaking multiple numerical simulations were conducted, with different ratios between the front and rear length of the crest. Glasbergen (2017) concluded that only the front part L_ξ of the wave is of interest for the type of wave breaking.

$$\xi_{tsunami,1D} = \frac{\tan(\alpha_2)}{\sqrt{\frac{H_\xi}{L_\xi}}} \tag{ 2 }$$

where α_2 is the slope of the continental shelf, H_ξ and L_ξ are the wave height and the wave front length at a depth of 100 m, respectively (see Figure 3). The choice of a 100 m depth is based on the parameter used by ASCE (2016). Essentially, at a depth of 100 m the wave is close to the coast, but the behaviour is still rather linear and non-breaking.

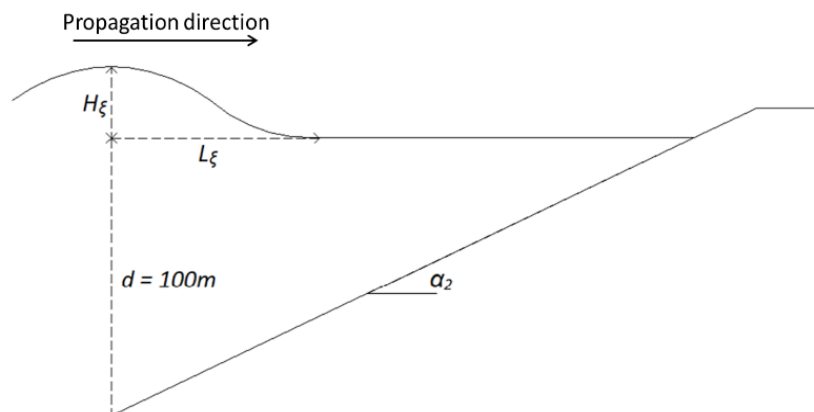


Figure 3: Relevant parameters to describe the wave breaking of a tsunami (Glasbergen, 2017).

The adapted surf-similarity parameter (see eq. (2)) was defined for an infinitely wide coast. For a coastline with narrow bays, like the Sanriku coastline, a tsunami parameter $\xi_{tsunami}$ that includes 2D bay effects was proposed. For this, a factor β is inserted into the definition of the surf-similarity parameter. For the case where the coastline can be schematized as a 1D model, β would be equal to 1, and in other places where 2D effects become relevant β will describe the shape of the bay. Conservation of energy dictates that the energy will increase by an additional factor W_b/W_h due to the narrowing of the bay in the absence of dissipation, and that therefore the wave height will increase by a factor $\sqrt{W_b/W_h}$.

The part of interest for 2DH simulations is the nearshore area, which is indicated as the simulation area in Figure 4. The bay is schematized as having linearly converging vertical walls and a constant bed slope, which is equal to the slope of the continental shelf and therefore equal to α_2 , as indicated in Figure 5. The width at the bay entrance is W_b , and the width at the coastline is W_h .

Shimozono (2016) shows that the two-dimensional linear shallow water equations can be reduced to one-dimensional wave equations under the assumption of small transverse flow acceleration for a sufficiently small ratio of bay width to wavelength. Otherwise the wave behaviour becomes two-dimensional and could even cause total reflection.

As the surf-similarity parameter is based on the wave conditions at 100 m depth, but wave breaking occurs with an increased wave height that is influenced by the reduced width of the bay, it is postulated that the wave height in equation (3) should be replaced by $\sqrt{\beta}H_\xi$, where the bay factor $\beta=W_b/W_h$ is used to describe the type of wave breaking in bays. The proposed tsunami surf-similarity parameter is therefore given by eq. (3). It has to be stated that the use of the factor β is only valid for a certain range of bay shapes. For a V-shaped bay the factor β goes to infinity, which makes the equation invalid. The applicable range of factor β for which eq. (3) is valid is explained later in this paper.

$$\xi_{tsunami} = \frac{\tan(\alpha_2)}{\sqrt{\frac{\sqrt{\beta}H_\xi}{L_\xi}}} \quad \text{where } \begin{cases} \beta = 1 \text{ for straight coastlines} \\ \beta = \frac{W_b}{W_h} \text{ for indented coastlines} \end{cases} \quad (3)$$

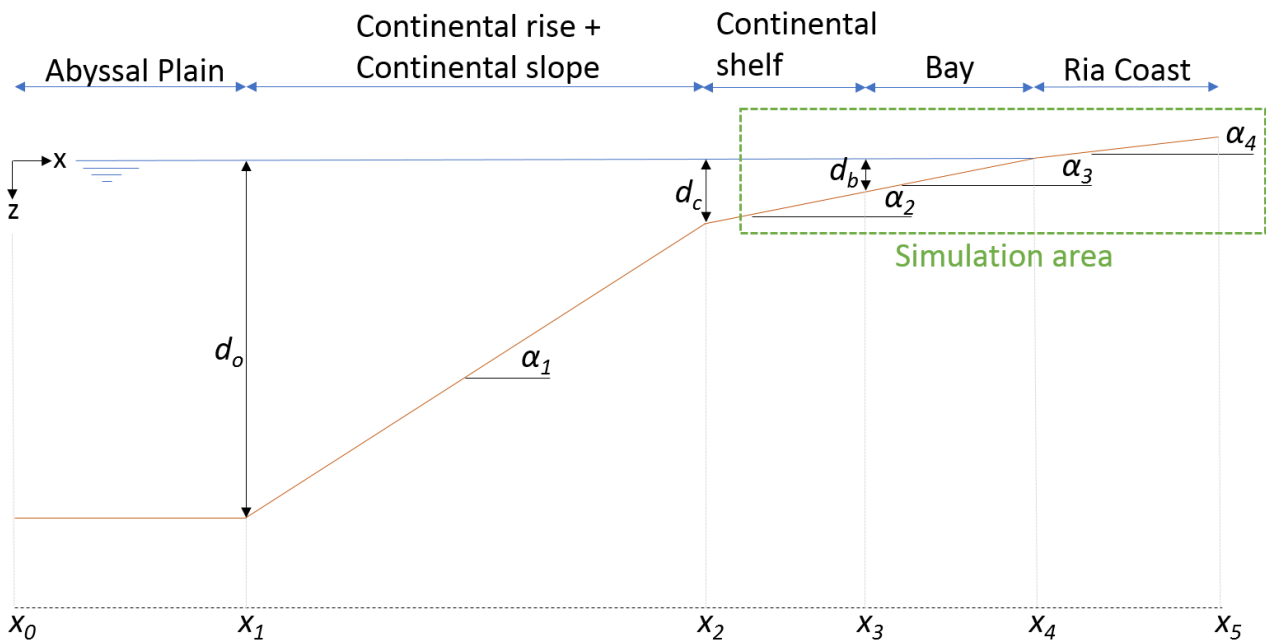


Figure 4: Schematization of the ocean bathymetry, where d_o , d_c and d_b are the depth offshore, at the edge of the continental shelf and at the bay mouth, respectively. α_1 , α_2 , α_3 and α_4 are the slopes of the continental rise, continental shelf, bay and inland topography, respectively.

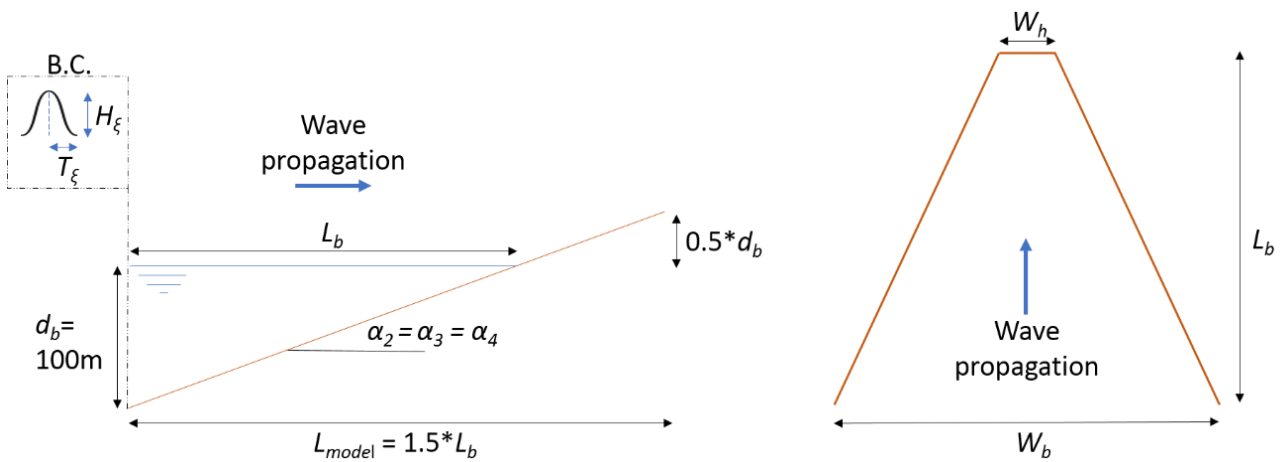


Figure 5: The schematization of a bay along the Sanriku coast (corresponding to the “simulation area” in Fig. 5), where d_b is the depth at the bay mouth which is set constant to 100 m, L_b the length of the bay, W_b the width of the bay mouth, W_h the width of the bay head and α_2 , α_3 and α_4 are the slopes of the continental shelf, bay and inland topography, respectively (and which are assumed to be equal).

2.2 Geometry of bays in the Tohoku region

This section will provide some insights into the characteristics of the simulation area and the different types of tsunami wave behaviour along the various characteristic geographies that make up the Tohoku coastline. However, the main focus will be on tsunami wave transformation in a ria coast embayment, which will then be compared with simulations of a tsunami approaching the gently sloping beaches that make up the straight coastline of the Sendai Plain (Glasbergen, 2017).

Table 1 gives an overview of the geometries of the bays along the Sanriku coastline (see Figure 6) and the bathymetry along the Sendai Plain, obtained by Navionics (2018) and the survey results of Shimozono et al. (2012).

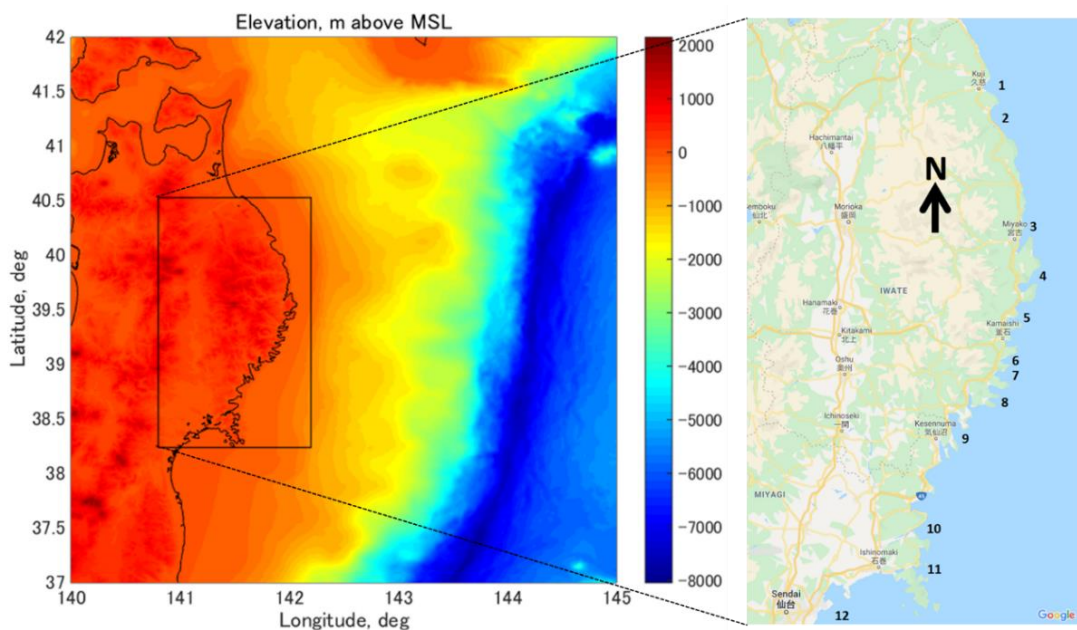


Figure 6: Left: Bathymetry of the Pacific Ocean offshore of the Tohoku region of Japan. Right: Location of the various points of the Sanriku and Sendai coast identified in Table 1 ©Google, 2019.

Table 1: Classification of the Tohoku coastline (Navionics, 2018; Shimonzono et al., 2012). Observed wave types are from Topics (2016, 2017, 2018).

Area	Bay Number	Location	Coast type	Observed wave type	Continental shelf slope (α_2)	Bay depth (d_b) [m]	Bay mouth width (W_b) [km]	Bay head width (W_h) [km]
North Sanriku	1	Kuji Bay	Ria coast	Breaking	1/160	40-60	5.5	2.5
	2	Noda Bay	Ria coast	Breaking	1/150	40-60	9.6	4.5
	3	Miyako Bay	Ria coast	Surging	1/145	60	3.5	1.4
Central Sanriku	4	Yamada Bay	Ria coast	Surging	1/90	80	3.0	3.0
	5	Otsuchi Bay	Ria coast	Surging	1/110	60	3	2.5
	6	Toni Bay	Ria coast	Surging	1/66	80	3.3	1.8
	7	Yoshima Bay	Ria coast	Surging	1/75	80	7.3	1.2
	8	Ryori Bay	Ria coast	Surging	1/88	60	3	1
South Sanriku	9	Hirota Bay	Ria coast	Surging	1/140	60	5.7	2.6
	10	Oppa Bay	Ria coast	Surging	1/104	60	6.5	6.5
	11	Onagawa Bay	Ria coast	Surging	1/120	60	5.0	5.0
Sendai Plain	12	Yuriage	Gentle sloped beach	Series of bores	1/590	-	-	-

2.3 Numerical model setup

To verify the ability of the parameter $\zeta_{tsunami}$ (eq. (3)) to discriminate between the different tsunami types, simulations were performed using the wave-resolving model SWASH (Simulating WAVes till SHore) (Zijlema et al., 2011). SWASH is a phase-resolving non-hydrostatic wave-flow model which is based on the vertically integrated, unsteady mass and momentum balance equations. The governing equations are the non-linear shallow water (NLSW) equations, including non-hydrostatic pressure. To simulate large-scale wave evolution and shallow water flows efficiently, the free-surface motion is tracked using a single-valued function, enabling the use of a relatively coarse resolution in the vertical.

Due to its limited free-surface tracking, SWASH cannot be directly applied to breaking waves, as essential processes such as overturning, air-entrainment and wave generated turbulence, are absent. However, if only the macro scale is relevant, the conservation of mass and momentum can be used to treat discontinuities in flow variables (free surface, velocities), and consequently to determine the bulk dissipation of broken waves and their associated energy losses due to their physical resemblance to (steady) bores (Smit et al., 2013). Besides bore dissipation, the initiation of the wave breaking process must be adequately described. Though the applied momentum balance inherently takes into account the balance between nonlinear steepening (enables wave shoaling) and frequency dispersion (corrects celerity of shoaling wave), this balance is a very delicate one, which places heavy demands on its accuracy through the required vertical resolution. For instance, the study of Smit et al. (2013) demonstrates that, at a relatively coarse vertical resolution (say one or two layers), the effect of vertical acceleration at the front face of the breaking wave is generally overestimated, and hence slows down the process of incipient wave breaking. Although a proper solution to this problem is to increase the number of vertical layers (to, say, twenty layers), this obviously incurs a computational burden that scales quadratically with the number of layers. As an alternative, Smit et al. (2013) proposed two breaking criteria that locally

impose a hydrostatic pressure distribution under the wave front and allow the persistence of wave breaking, respectively. A hydrostatic pressure is assumed at the front of the wave when it exceeds a certain wave steepness threshold, eq. (4). The threshold used in SWASH was based on flume experiments, and an α_s of 0.6 is proposed, which corresponds to a local front slope of 25°.

$$\frac{\partial \zeta}{\partial t} = \alpha_s \sqrt{gd} \tag{ 4 }$$

Note that SWASH automatically re-adapts the value of α_s to persist wave breaking if $\alpha_s < 0.6$ while the local steepness is still high enough ($\alpha_s > 0.3$). Based on experiences related to the transformation of gravity and infra gravity waves in coastal waters, it is suggested that these thresholds are rather universal for a broad range of bottom slopes, as they merely compensate the lack of model accuracy (Smit et al., 2013, Rijnsdorp et al., 2014, 2015). The present study essentially represents a first attempt to model tsunami transformation near shore using this wave breaking approach, and the SWASH simulations were used to investigate the influence of the initial wave and bathymetry characteristics on the transformation of a tsunami. Depth-integrated 1D and 2DH models were used to determine the influence of the continental shelf slope and the bay geometry, respectively. For all simulations, a surface elevation time series, eq. (5), was used as the incoming wave at the open boundary (see B.C. in Figure 5).

$$\eta_{B.C.} = H_\xi * \sin^2\left(\frac{\omega t}{2}\right) \quad \text{for } 0 < t < 2\pi/\omega \tag{ 5 }$$

where ω is the angular frequency given by $\omega = 2\pi/T$, H_ξ is the wave height and T is the wave period at 100 m depth. The values of H_ξ and T were based on the GPS buoy observations from GB802, obtained through the Nationwide Ocean Wave Information Network for Ports and Harbours (NOWPHAS), see Figure 7. Even though the full waveform during the 2011 tsunami was more complex than a simple sine curve, the initial approach of the wave is the only aspect covered in this study, and this initial approach can be well approximated by a sine curve fit to the observed nearshore waveform.

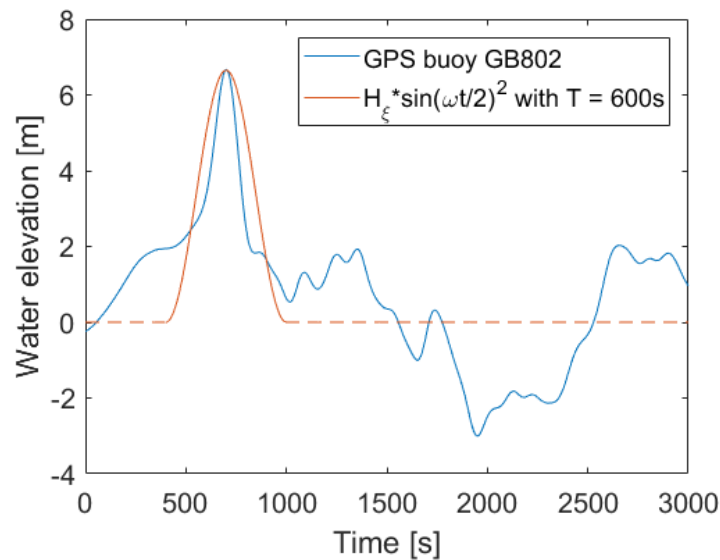


Figure 7: Comparison of an adjusted sinusoidal wave and the GPS buoy observations during the 2011 Tohoku Earthquake Tsunami.

The most important bathymetry parameter for the 1D simulations is the slope of the continental shelf (α_2), as shown in Figure 5, which is assumed to be equal to the slope of the bay and the inland topography ($\alpha_2 = \alpha_3 = \alpha_4$). The continental slope along the Tohoku coastline varies from 1/50 to 1/500.

Another important parameter is the bay geometry, which was included in the 2DH simulations. These 2DH simulations were conducted for a continental slope in the range of 1/50 to 1/100, since they cover the typical slopes along the Sanriku coastline. The depth at the bay mouth (d_b) stayed constant at a depth of 100 m for all simulations.

The schematized parameters of the bay can be changed one by one to see their influence on the characteristics of the tsunami wave. Based on the given bathymetry and geometry given in Table 1, and the wave buoy observations, the parameters in Table 2 were used to simulate different tsunami waves along the Tohoku coastline. The wave period T is used to obtain the water surface elevation time series of eq. (3). To obtain the wave front length L_{ξ} , linear theory is used: $L_{\xi} = \frac{1}{2} cT_{100} = \frac{1}{2} \sqrt{gd}T_{100}$ where d is 100 m.

Table 2: Parameters used for the SWASH simulations in this research. *The slopes are based on the range of continental shelf slopes along the Sendai Plain (1D) and the Sanriku coast (2DH).

Parameter	1D model	2DH model
Wave height H_{ξ} [m]	4,6 and 8	4,6 and 8
Wave period T_{100} [s]	600 and 1200	600 and 1200
*Continental shelf slope α_2 [-]	1/50, 1/75, 1/100, 1/150, 1/200, 1/300 and 1/500	1/50, 1/75 and 1/100
Bay mouth width W_b [m]	-	2000, 3000, 4000, 5000 and 6000
Bay head width W_h [m]	-	500, 1000, 1500, 2000, 2500 and 3000

To analyze different tsunami types at the coastline, a tailored Froude number Fr_{coast} is employed, given by eq. (6), where $u_{max,coast}$ is the maximum velocity at the coastline during inundation and h_{coast} is the water level at the moment of maximum velocity. Another important value is the maximum momentum flux $(hu^2)_{max}$ at the coastline during inundation, since this is an important parameter to determine the hydrodynamic forces on a given coastal structure (FEMA, 2012).

$$Fr_{coast} = \frac{u_{max,coast}}{\sqrt{gh_{coast}}} \quad (6)$$

3 Results

3.1 Validation of wave breaking

A validation was carried out by comparing wave breaking in SWASH with the results of Grilli et al. (1997), where the shoaling and breaking criterion of solitary waves was investigated on several slopes. Even though solitary waves might not be analogous to an actual tsunami (Madsen and Fuhrman, 2008), the tests of Grilli et al (1997) include the important processes of both nonlinearity and dispersion, which are critical to the range of breaker types the present research attempts to reproduce. For this, they used a fully nonlinear wave model, and computed the wave transformation on slopes of 1/100 to 1/8 and wave heights of 0.2, 0.4 and 0.6 m at a water depth of 1 m, using a time step of 0.01 s and a grid size of 0.1 m. The authors attempted to reproduce the computational results of Grilli et al. (1997) using SWASH, with Table 3 showing the results of this comparison, where the breaking height (H_b), the breaking depth (h_b) and the breaking location (x_b) are given.

Table 3: Breaker height (H_b), breaker depth (h_b) and breaker location (x_b) for the tests by Grilli et al. (1997) and the SWASH simulations carried out for the present study.

Slope	Tests (Grilli et al. 1997)				SWASH			Difference
	H_0 [m]	H_b [m]	h_b [m]	x_b [m]	H_b [m]	h_b [m]	x_b [m]	x_b [%]
1/100	0.2	0.36	0.34	66	0.32	0.45	55.4	16.1
	0.4	0.63	0.60	39	0.48	0.66	33.8	13.3
	0.6	0.78	0.76	24	0.60	0.81	18.9	21.30
1/35	0.2	0.36	0.25	26	0.28	0.36	22.4	13.9
	0.4	0.59	0.43	20	0.46	0.58	14.6	27.0
	0.6	0.75	0.57	15	0.58	0.74	9	40.0
1/8	0.2	-	-	-	0.23	0.18	6.6	-
	0.4	0.41	0.08	7.4	0.41	0.41	4.7	36.5
	0.6	0.59	0.13	7	0.55	0.56	3.5	50.0

The results of the SWASH simulations correlate well with the tests of Grilli et al. (1997), with Figure 8 showing an example of a test with a slope of 1/35 and H_0 of 0.2 m. Up to $x/h_0 = 22.5$, the results for SWASH and Grilli et al. (1997) are similar. After that, the wave in SWASH starts to dissipate energy and drops in wave height, in contrast to Grilli et al. (1997), where the plunging breaking starts, which is not explicitly modelled in SWASH.

Essentially, the waves in the SWASH simulations break in slightly deeper water compared to those in Grilli et al. (1997), and this difference is larger for steeper slopes. For the 1/8 slope, the location of wave breaking in SWASH is quite far offshore, whereas for the mild slopes the SWASH simulations results compare well with Grilli et al. (1997). This mismatch in the location of breaking can be explained by the fact that in SWASH this happens when the slope of the free surface is larger than the factor $\alpha_s = 0.6$, as explained earlier. The breaking in Grilli et al. (1997) starts when a vertical tangent is reached, which is never the case in SWASH.

To check whether the bottom friction has any influence, a simulation was conducted where the default Manning value of $0.019 \text{ m}^{-1/3}\text{s}$ was decreased to $0.01 \text{ m}^{-1/3}\text{s}$. However, there was no significant effect on the breaking location in SWASH.

The present research considers only mild slopes, where SWASH performed well.

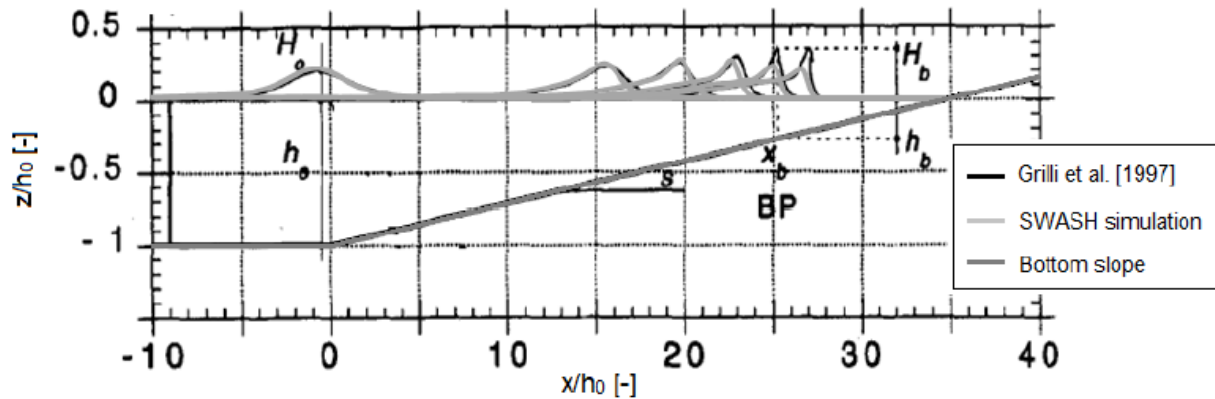


Figure 8: Solitary wave breaking tests: Results of Grilli et al. (1997) vs SWASH simulations. For an offshore wave height (H_0) of 0.2 m, an offshore depth (h_0) of 1.0 m, a slope (s) of 1/35, a breaker height (H_b) of 0.36 m, a breaking depth (h_b) of 0.25 m, and the location of breaking (x_b) of 0.26 m.

3.2 Maximum momentum flux and tsunami wave type (1D model)

A relationship was found between the maximum momentum flux at the coastline and the slope, see Figure 9. As the wave height increases, $(hu^2)_{max}$ also increases. For the wave period, the opposite relationship applies. When the wave period increases, $(hu^2)_{max}$ at the coastline decreases, except for the mildest slope 1/500. So, the maximum momentum flux depends on the slope and the wave period. For simulations with $T_{100} = 600 \text{ s}$, the maximum momentum flux is reached for a slope of 1/300. When T_{100} is increased to 1200 s, the maximum occurs for slopes for a milder slope (1/500 for this input parameters). This can be explained by the fact that for shorter waves, breaking occurs earlier than for longer waves (with similar wave heights and slopes).

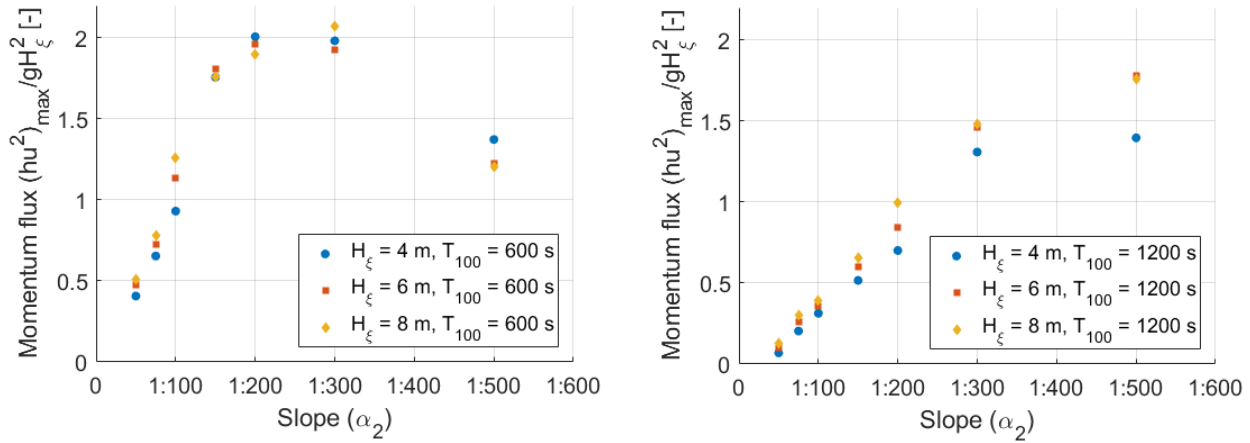


Figure 9: The slope of the continental shelf (α_2) vs. the maximum momentum flux at the coastline $(hu^2)_{\max}$ divided by (gH_ξ^2) to make it dimensionless, for three different wave heights (H_ξ) and two different wave front periods (T_{100}) at a depth of 100 m. Left: $T_{100} = 600$ s. Right: $T_{100} = 1200$ s.

Tsunami wave fronts obtained from the simulations were then classified into three different types; non-breaking wave (surging), breaking wave front and undular bore breaking. The wave front is called ‘breaking’ (either for breaking front and undular bore breaking) for simulations where the wave steepness (α_s) exceeded 0.6 (initiating wave breaking) or 0.3 (persistence of wave breaking after incipient breaking), and so the non-hydrostatic effects have been removed by SWASH to speed up or to persist the breaking process. It should be noted that breaking-induced dissipation is not determined by the switch based on α_s , and is solely resolved by the mass and momentum conservations (Zijlema and Stelling, 2008). The transition between a breaking wave front and undular bore formation is obtained by visual observations of the simulation results. Figure 10 shows this clear distinction in wave types where, in the rightmost picture, small amplitude undulations can be seen on top of the wave.

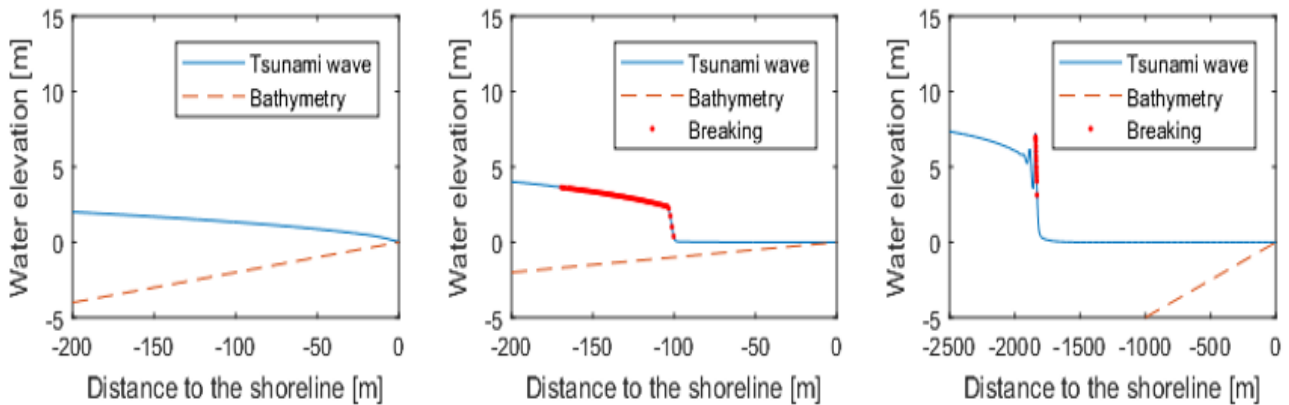


Figure 10: Different wave front types. B.C.: timeseries $H_\xi = 6$ m and $T_{100} = 600$ s. Left to right: Continental shelf slope (α_2) 1/50: Non-breaking (surging) wave, 1/100: Breaking wave front, 1/200: Undular bore breaking. The red dots indicate the area where the wave breaking process is ongoing, determined by the SWASH simulations.

The tsunami surf-similarity parameter $\zeta_{tsunami,1D}$, which is the surf-similarity parameter without the influence of the bay geometry ($\beta = 1$), was plotted against the Froude number at the coastline Fr_{coast} and the maximum momentum flux at the coastline in Figure 11. This shows that there is a clear distinction between the three different wave types. The boundary between a surging wave and a breaking front is $\zeta_{tsunami,1D} = 0.54$, and between a breaking front and undular bore breaking is $\zeta_{tsunami,1D} = 0.27$. It can also be observed that the Froude number (Fr_{coast}) and the maximum momentum flux $(hu^2)_{\max}$ at the coastline increases when tsunami waves break, and even more when undular bore breaking occurs, which is related to a decreasing $\zeta_{tsunami,1D}$. To summarize, the following ranges of $\zeta_{tsunami,1D}$ that correspond to the different wave types can be discerned:

$\xi_{tsunami,1D} < 0.27$: Undular bore breaking
 $0.27 < \xi_{tsunami,1D} < 0.54$: Breaking wave front
 $\xi_{tsunami,1D} > 0.54$: Non-breaking wave front (surging)

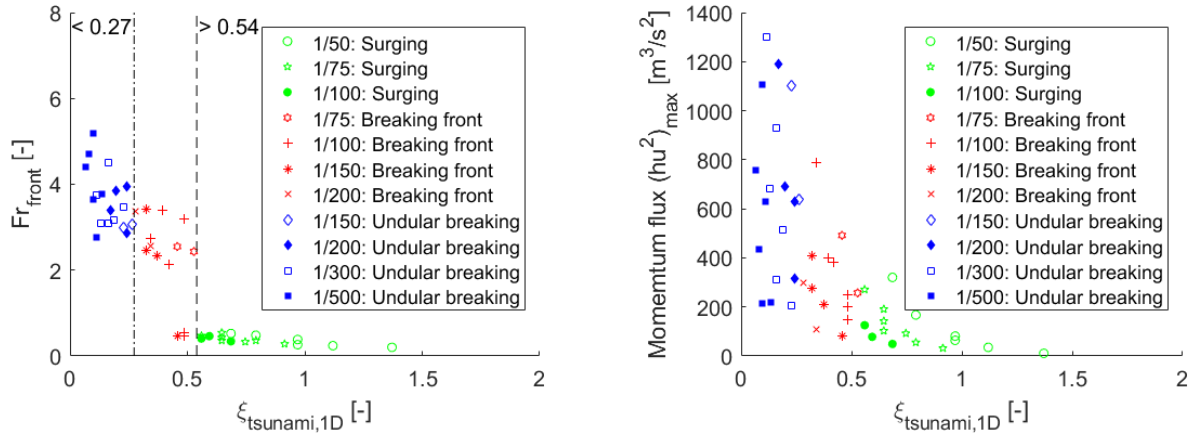


Figure 11: Surf-similarity parameter $\xi_{tsunami,1D}$ vs maximum Froude number $F_{r_{coast}}$ and maximum momentum flux $(hu^2)_{max}$ at the coastline.

Figure 12 shows a scatter plot of the simulation results and the trend lines for the location of undular bore formation, undular bore breaking and single wave front breaking. For the simulations conducted, the undulations of undular bores always finally break when they get close enough to the shoreline. The coefficient of determination R^2 is a statistical measure that indicates the coherence between the data and the trendline (the closer R^2 to 1.00, the better the correlation).

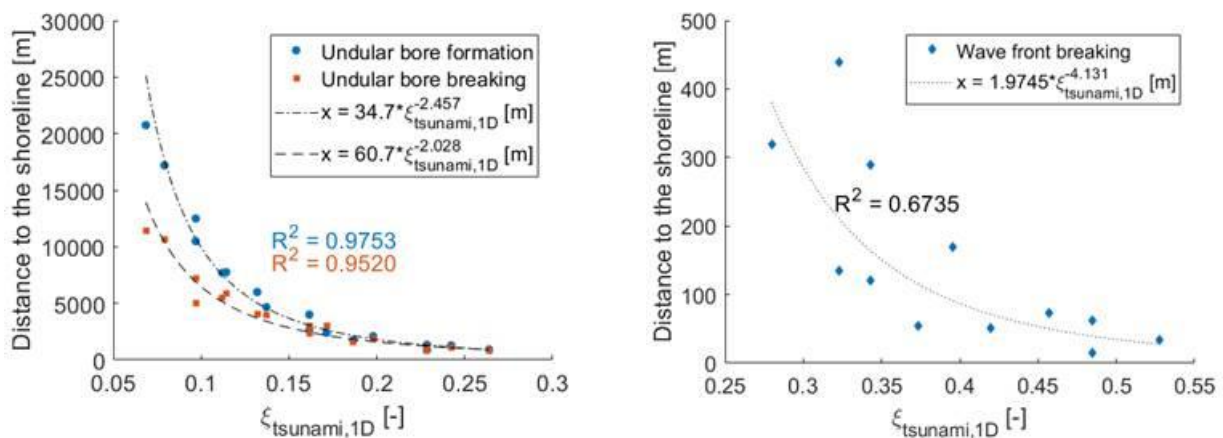


Figure 12: Empirical fitting to obtain formulas to predict the location of undular bore formation, undular bore breaking and single wave front breaking. R^2 is the coefficient of determination.

3.3 Bay geometry (2DH model)

The indented coastline along the Sanriku coast ensures that 2D effects such as wave amplification become important in the nearshore area. 2DH simulations were performed to provide more insights into the influence of different bay geometries on the transformation of a tsunami wave front. Figure 12 gives an example of a simulation where $\alpha_2 = 1/100$, $W_b = 3000$ m, $W_h = 1500$ m, $H_\xi = 6$ m and $T_{100} = 600$ s. Figure 13, a slightly curved wave crest can be seen near the boundaries of the bay, due to the stepwise angular grid. However, the wave crest in the middle of the bay remains rather straight. Therefore, the results obtained in the following simulations were based on the output values in the middle of the bay, given by the red dashed line in the leftmost picture of Figure 13.

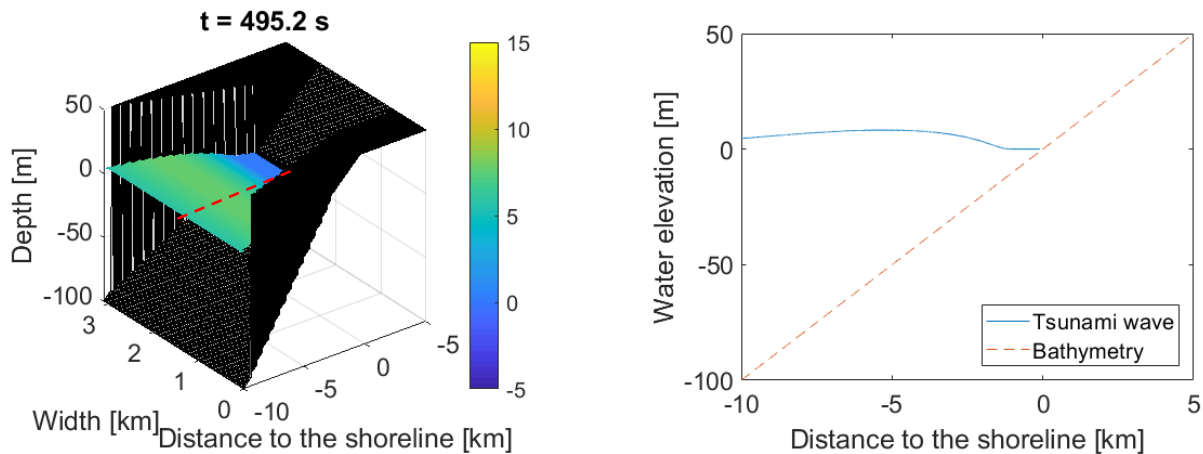


Figure 12: Example of the surface elevation at $t = 1750.5$ s from a 2DH SWASH simulation. Left: 3D view, red dashed line indicates the section of the 1D plot. Right: Plot of the section indicated by the red dashed line.

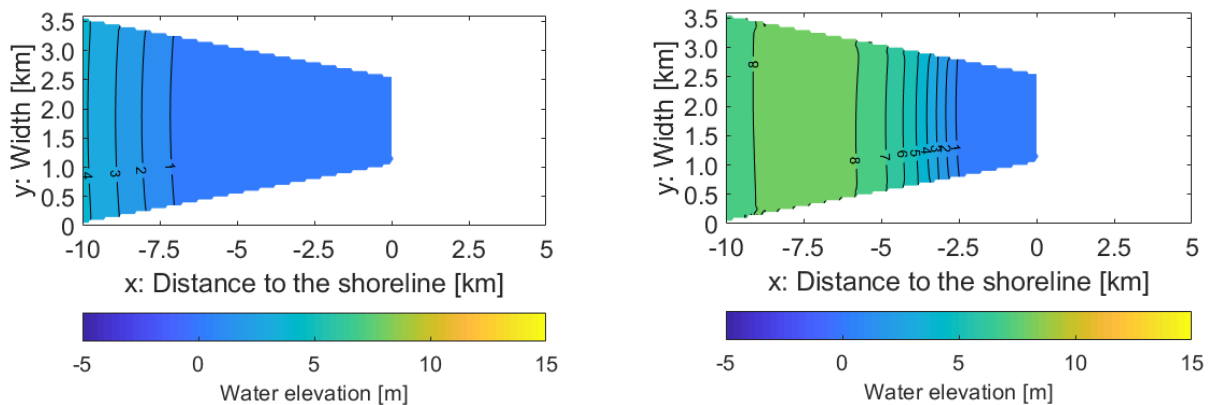


Figure 13: Top view of a 2DH simulation, where the 2D effects near the boundaries are visible. Left: At $t = 1550.3$ s. Right: At $t = 1750.5$ s.

The authors hypothesized that the narrowing of the bay, which should influence the amplification of the wave, determines to a large extent the transformation of the tsunami waves. To test the validity of this hypothesis several 2DH simulations were conducted with varying bay geometries, which are given in Table 4. Since the depth at the bay mouth was set constant at a depth of 100 m, the bathymetry parameters that change along the Sanriku coast are the width of the bay mouth (W_b) and the width of the bay head (W_h).

Simulations 8, 10, 11 and 12 (see Table 4) show the influence of a change in W_b . The funneled shaped geometry of the bay amplifies the tsunami wave and therefore the steepness of the wave increases. The larger the bay mouth opening, with a constant bay head width, the larger this amplification factor becomes, and the earlier the wave front will break.

The effect of a changing W_h is the same but opposite to the change in W_b . Simulations 8 (1D: $W_b = W_h$), 9, 11, 13 and 14 show the influence of a change in W_h . When W_h increases, the amplification of the wave decreases and therefore the steepness decreases. The tsunami wave will break at a later stage.

Simulations 11, 15, 16 and 18 have the same bay shape factor β , which is defined as the W_b/W_h ratio, same offshore wave characteristics but different values of W_b and W_h . The breakpoint location, the Froude number and the maximum momentum flux at the coastline are approximately equal for these simulations. This corroborates the hypothesis that β is an important parameter for tsunami wave transformation in bays. An interesting conclusion can be made when comparing simulations 6 and 7, where the only parameter that changes is β . Simulation 6 is a 1D simulation ($\beta = 1$) and simulation 7 is a 2DH simulation (where bay geometry is included, $\beta = 2$). The wave type at the coastline is different. A surging wave was observed in the simulation without the influence of bay geometry, and a breaking wave when the effect of the narrowing of the bay was included. This indicates that bay geometry influences the type of tsunami wave along the Tohoku coastline and that a shape factor β needs to be included in the tsunami surf-similarity parameter.

Table 4: 2DH simulations: Influence of the bay geometry (β) on the tsunami wave transformation.

*) 1D simulations, without the influence of bay geometry. The type of wave at each location was established by the authors by visual inspection of Topics (2016, 2017, 2018).

Simulation Number	α_2	L_ξ [m]	H_ξ [m]	W_b [m]	W_h [m]	β [-]	Wave type	Breakpoint [m]	Fr_{coast} [-]	$(hu^2)_{max}$ [m ³ /s ²]
1*	1/50	9396.28	6	-	-	1.00	Surging	None	0.48	167.31
2	1/50	9396.28	6	3000	1500	2.00	Surging	None	1.29	332.95
3	1/50	9396.28	6	3000	2500	1.20	Surging	None	1.18	254.23
4*	1/50	9396.28	8	-	-	1.00	Surging	None	0.52	320.4
5	1/50	9396.28	8	3000	1500	2.00	Surging	None	1.26	317.17
6*	1/75	9396.28	4	-	-	1.00	Surging	None	0.54	102.61
7	1/75	9396.28	4	3000	1500	2.00	Breaking front	60	1.28	142.12
8*	1/75	9396.28	6	-	-	1.00	Breaking front	34	2.43	257.15
9	1/75	9396.28	6	3000	2000	1.50	Breaking front	61	1.36	387.10
10	1/75	9396.28	6	2000	1500	1.33	Breaking front	58	1.19	332.05
11	1/75	9396.28	6	3000	1500	2.00	Breaking front	85	1.36	490.87
12	1/75	9396.28	6	4000	1500	3.00	Breaking front	88	1.23	654.05
13	1/75	9396.28	6	3000	1000	3.00	Breaking front	105	1.40	675.55
14	1/75	9396.28	6	3000	500	6.00	Breaking front	125	1.37	678.19
15	1/75	9396.28	6	4000	2000	2.00	Breaking front	75	1.38	488.05
16	1/75	9396.28	6	5000	2500	2.00	Breaking front	80	1.21	501.32
17	1/75	9396.28	6	5000	3000	1.67	Breaking front	68	1.37	405.97
18	1/75	9396.28	6	6000	3000	2.00	Breaking front	80-85	1.38	475.91
19	1/75	14094.41	6	3000	1500	2.00	Surging	None	0.77	344.09
20	1/75	18792.55	6	3000	1500	2.00	Surging	None	0.78	178.91
21	1/75	9396.28	8	-	-	1.00	Breaking front	74	2.55	491.56
22	1/75	9396.28	8	3000	1500	2.00	Breaking front	150	1.43	961.45
23	1/100	9396.28	4	3000	1500	2.00	Breaking front	14.5	0.58	240.85
24	1/100	9396.28	6	-	-	1.00	Breaking front	170	3.39	399.74
25	1/100	9396.28	6	3000	1500	2.00	Breaking front	280	1.56	870.94
26	1/100	9396.28	8	-	-	1.00	Breaking front	290	2.62	789.69

Figure 14 shows the Froude number at the coast for all 2DH simulations against the tsunami surf-similarity parameter defined in eq. (3), which includes the influence of the bay geometry thanks to the inclusion of β .

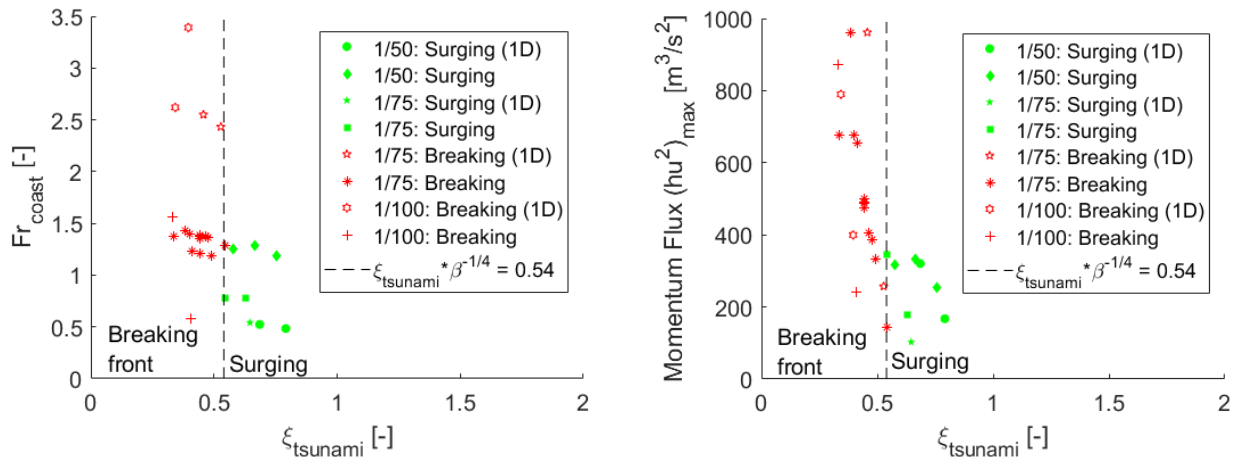


Figure 14: Final tsunami surf-similarity parameter ($\xi_{tsunami}$) vs. Froude number (Fr_{coast}) and maximum momentum flux $(hu^2)_{max}$ at the coastline.

The final proposed parameter $\xi_{tsunami}$, given in eq. (3), was plotted against the Froude number and the maximum momentum flux at the coastline for all 2DH simulations in Figure 14. A clear distinction between a surging wave and a breaking wave front is obtained:

$$\begin{aligned}
 (2DH: 1 < \beta < 6) \quad \xi_{tsunami} \leq 0.54: & \quad \text{Breaking wave front} \\
 \xi_{tsunami} > 0.54: & \quad \text{Non-breaking wave front (surging)}
 \end{aligned}$$

3.4 Validation of the proposed surf similarity parameter

To check if the proposed method can be used for real-life prediction of tsunami wave types along the Tohoku coastline, the authors attempted to validate it against Youtube video observations of the *2011 Tohoku Earthquake Tsunami*. 12 different locations, as shown in Figure 6, were used to check if the wave type along the coastline can be predicted by using $\xi_{tsunami}$, with or without the bay shape factor β . The results are summarized in Table 5.

For the 1D prediction (eq. (2)), four out of the 12 locations are predicted incorrectly. However, only two out of the 12 predictions were incorrect when using the new proposed parameter (eq. (3)) that included the actual β of each bay. The incorrect prediction for Miyako Bay can probably be explained by the fact that the direction of the incoming tsunami wave was very different to that in other bays. Figure 6 shows that the opening of the Miyako Bay is directed to the north-east, whereas the tsunami wave arrived from the south-east. Since tsunami directivity can have an influence on breaking type, future research should include this variable into the analysis. The authors could not find any explanation for the incorrect prediction in Hirota Bay. Since the bay slope is gentle and the narrowing effect of the bay is small a breaking wave front was expected, in contrast to the observations during the *2011 Tohoku Earthquake Tsunami*.

Table 5: Case study 2011 Tohoku Earthquake Tsunami. *Italic text*: Incorrect predictions. Underlined text: Correct predictions due to bay geometry influence, after a wrong prediction without considering bay geometry influence. Observed wave types are from Topics (2016, 2017, 2018).

Nr.	Location	β	H_ξ	T_ξ	L_ξ	$\xi_{tsunami,1D}$	Prediction 1D	$\xi_{tsunami}$	Prediction 2DH	Observed wave type
1	Kuji Bay	2.20	4.20	300	9396	0.30	Breaking front	0.20	Breaking front	Breaking front
2	Noda Bay	2.13	4.20	300	9396	0.32	Breaking front	0.22	Breaking front	Breaking front
3	Miyako Bay	2.50	4.20	300	9396	0.33	<i>Breaking front</i>	0.21	<i>Breaking front</i>	Surging
4	Yamada Bay	1.00	6.80	900	28189	0.72	Surging	0.72	Surging	Surging
5	Otsuchi Bay	1.20	6.80	900	28189	0.59	Surging	0.53	Surging	Surging
6	Toni Bay	1.83	6.80	900	28189	0.98	Surging	0.72	Surging	Surging
7	Yoshima Bay	6.08	6.80	900	28189	0.86	<i>Surging</i>	0.35	<u>Breaking front</u>	Breaking front
8	Ryori Bay	3.00	6.80	900	28189	0.73	<i>Surging</i>	0.42	<u>Breaking front</u>	Breaking front
9	Hirota Bay	2.19	6.40	900	28189	0.47	<i>Breaking front</i>	0.32	<i>Breaking front</i>	Surging
10	Oppa Bay	1.00	6.40	900	28189	0.62	Surging	0.62	Surging	Surging
11	Onagawa Bay	1.00	6.40	900	28189	0.55	Surging	0.55	Surging	Surging
12	Yuriage	-	6.00	900	28189	0.12	Undular breaking	-	-	Undular breaking (series of bores)

4 Discussion

After conducting multiple 1D and 2DH simulations, a distinction could be made between different types of tsunami waves. The proposed tsunami surf-similarity parameter for 1D situations provides a distinction between three different tsunami wave types (Figure 11), where the surf-similarity parameter for 2DH simulations only allows to distinguish between two different wave types (Figure 14). This is due to the range in continental shelf slopes (α_2) being much larger for the 1D simulation than for the 2DH simulations, resulting in a smaller range of surf-similarity parameters. Since undular bore breaking most likely occurs with shallow continental shelf slopes, a distinction between three wave types should be obtained by increasing the number of 2DH simulations with shallower slopes (1/50 – 1/500).

For most tsunami events, both the frequency dispersion and nonlinearity effects are small and can be neglected during offshore propagation (Liu, 2009). Therefore, linear wave theory can be used as a first approximation to calculate changes in tsunami wave height as it moves across an ocean (Bryant 2014). Green's Law is a classic linear theory that describes shoaling, and which can be applied for cases where the depth varies slowly (Lipa et al. 2016). Glasbergen (2017) compared wave buoy measurements near Sendai, during the 2011 Tohoku Earthquake Tsunami, with the results of a 1D SWASH model and with Green's Law approximation. In the present research, similar simulations were conducted to compare the SWASH results with an approximation of Green's Law and buoy observations near Kamaishi Bay, extending the applicability of the results of Glasbergen (2017) to the ria coastline in the Northern area of Tohoku. These results can be seen in Figure 15.

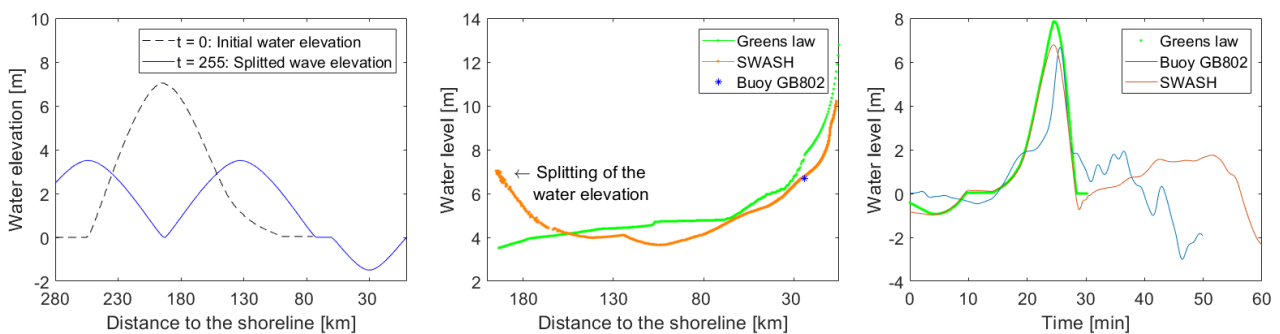


Figure 15: Left: decomposition of a simplified 2011 Tohoku tsunami initial condition into traveling waves. Middle: highest water elevation as calculated in 1D calculations with the initial (still) water level and bed topography on the transect between the tsunami epicenter of the wave buoy near Kamaishi bay. The 1D calculations over this transect were obtained using both SWASH and Green's Law. Right: the time series of water elevation as calculated at the buoy near Kamaishi bay, which is indicated by the black triangle near the coastline on the blue transect in the left plot. The water elevation is again calculated with SWASH and Green's Law, and also compared to the results of the buoy near Kamaishi bay. Results are from Roubos (2019).

Before the point of breaking, Green's Law seems to agree rather well with both the buoy observations and the SWASH calculation. This implies that 1D linear wave theory can be used to shoal the measured wave height to 100 m depth and calculate the associated wavelength to use in the proposed tsunami parameter $\xi_{tsunami}$, at least for the continental shelf bathymetry as found at the Tohoku coast. However, since Green's Law is a 1D analytical solution, this approach only seems to be valid for coastal regions near the epicenter of the earthquake. To predict offshore tsunami wave transformation for locations more northwards or southwards of the earthquake, 2D or 3D modelling should be applied.

5 Conclusions

Multiple depth-integrated numerical simulations were conducted to find a relationship between wave characteristics, bathymetry parameters and the type of tsunami wave breaking. A newly defined surf similarity parameter for tsunamis $\xi_{tsunami}$ (eq. (7)) can be used to obtain an extra insight into tsunami wave transformation inside a bay. The parameter describes the steepness of the front of the wave and includes the relative contraction of the bay, and can be used to predict the type of wave breaking. Three types of breaking can occur according to different values of the parameter: undular bore breaking, a breaking wave front and a non-breaking (surging) wave front. These wave types occur for a gentle, an

intermediate and a steep continental shelf, respectively. The first classification is based on 1D simulations where there is no bay along the coast ($\beta = 1$), with a continental slope (α_2) in the range of 1/50 to 1/500. The second classification is based on 2DH simulations where bay geometry plays a role along the coastline ($1 < \beta < 6$), with a continental slope in the range of 1/50 to 1/100.

$$\xi_{tsunami} = \frac{\tan(\alpha_2)}{\sqrt{\frac{\beta H_\xi}{L_\xi}}} \quad \text{where} \quad \begin{cases} \beta = 1 \text{ for straight coastlines} \\ \beta = \frac{W_b}{W_h} \text{ for indented coastlines} \end{cases} \quad (7)$$

(1D: $\beta = 1$)	$\xi_{tsunami} < 0.27$:	Undular bore breaking
	$0.27 < \xi_{tsunami} < 0.54$:	Breaking wave front
	$\xi_{tsunami} > 0.54$:	Non-breaking wave front (surging)
(2DH: $1 < \beta < 6$)	$\xi_{tsunami} \leq 0.54$:	Breaking wave front
	$\xi_{tsunami} > 0.54$:	Non-breaking wave front (surging)

The resulting breaker type is of critical importance in the design of coastal structures because of the differing forces exerted on structures by non-breaking vs. breaking waves. Forces due to non-breaking waves can be parameterized by the Morrison equation for moored structures or by conservation of momentum for waves reflecting off of founded structures. For breaking waves, however, empirical methods such as those of Sainflou (1928), Goda et al. (1966), or de Almeida et al. (2020) become necessary.

Acknowledgements

The authors would like to express sincere gratitude to the Delft Deltas, Infrastructures & Mobility Initiative (DIMI), which made it possible to do research in Japan. A multidisciplinary group from the Delft University of Technology and the University of Tokyo and Waseda visited Otsuchi Town to learn lessons from the reconstruction of the Japanese coasts destroyed by the tsunami in 2011. A special thanks to the Delft University of Technology and Waseda University, which contributed to this research and offered their research facilities. A part of the present work was performed as activities of the Research Institute of Sustainable Future Society, Waseda Research Institute for Science and Engineering, Waseda University.

Author contributions (CRediT)

JJR: Simulations, analysis of results, writing original draft. TG: Simulations, analysis of results. BH: Analysis of results, overall research formulation and guidance, writing of draft. JDB: Analysis of results, overall research formulation and guidance, writing of draft. MZ: Writing of draft, review and editing. ME: Writing of draft, review and editing. MFST: Review and editing.

Notations

Name	Symbol	Unit
Seaward slope of the structure in the Iribarren formula [-]	α	-
Slope of the continental rise [-]	α_1	-
Slope of the continental shelf [-]	α_2	-
Slope of the bay [-]	α_3	-
Slope of the inland topography [-]	α_4	-
Wave steepness [-]	α_s	-
Bay shape factor [-]	β	-
Wave celerity [m/s]	c	m/s

Depth [m]	d	m
Depth at the bay mouth [m]	d_b	m
Depth at the edge of the continental shelf [m]	d_c	m
Offshore depth [m]	d_o	m
Dissipative parameter [-]	D	-
Hydromagnetic force [kN]	F_d	kN
Hydrostatic force [kN]	F_h	kN
Impulsive force [kN]	F_s	kN
Tailored Froude number for tsunami-waves [-]	Fr_{coast}	-
Gravitational acceleration [m/s^2]	g	m/s^2
Water level [m]	h	m
Breaking depth [m]	h_b	m
Water level at the moment of maximum velocity [m]	h_{coast}	m
Offshore depth [m]	h_o	m
Maximum momentum flux [m^3/s^2]	$(hu^2)_{max}$	m^3/s^2
Wave height [m]	H	m
Breaking height [m]	H_b	m
Wave height at deep water [m]	H_o	m
Wave height at a depth of 100m [m]	H_ξ	m
Length of the bay [m]	L_b	m
Length of the numerical model [m]	L_m	m
Deep-water wavelength [m]	L_o	m
Wave front length at a depth of 100m [m]	L_ξ	m
Surface elevation time series as boundary condition in the numerical model [m]	$\eta_{B.C.}$	m
Coefficient of determination [-]	R^2	-
Slope [-]	s	-
Time [s]	t	s
Wave period [s]	T	s
Wave front period [s]	T_{100}	s
Wave front period [s]	T_ξ	s
Velocity [m/s]	u	m/s
Maximum velocity at the coastline [m/s]	$u_{max,coast}$	m/s
Width of the bay entrance [m]	W_b	m
Width of the bay head [m]	W_h	m
Distance [m]	x	m
Wave breaking location [m]	x_b	m
Angular frequency [rad/s]	ω	rad/s
Iribarren number [-]	ξ	-
Tsunami surf-similarity parameter [-]	$\xi_{tsunami}$	-
1D Tsunami surf-similarity parameter [-]	$\xi_{tsunami,1D}$	-

References

- Árnason, H. (2005). Interactions between an Incident Bore and a Free-Standing Coastal Structure. Washington: Doctoral dissertation.
- ASCE. (2016). Chapter 6: Tsunami Loads and effects. In ASCE, ASCE 7 Standard, Minimum Design Loads and Associated Criteria for Buildings and Other Structures (pp. 25-50). Reston: American Society of Civil Engineers.
- Battjes, J. A. (1974) "Surf Similarity", Coastal Engineering Proceedings.

- Benjamin TB and Lighthill, MJ. 1954. On cnoidal waves and bores. Proceedings of the Royal Society of London. Series A, Mathematical and Physical Sciences, Vol. 224, No. 1159, pp. 448-460.
- Binnie, A. M. and Orkney, J. C. (1955) “Experiments on the flow of water from a reservoir through an open horizontal channel II: The formation of hydraulic jump”. Proceeding of Royal Society of London, Series A, 230, 1181, 237-246.
- Bonneton, P., Bonneton, N., Parisot, J.-P. and Castelle, B. (2015) “Tidal bore dynamics in funnel-shaped estuaries”, *Journal of Geophysical Research: Oceans*, 120 (2), 923-941.
- Bryant, E. (2014) “Tsunami - The Underrated Hazard”, Chichester: Springer International.
- Bricker, J. D., & Nakayama, A. (2014). “Contribution of trapped air, deck superelevation, and nearby structures to bridge deck failure during a tsunami”. *Journal of hydraulic engineering*, 140(5), 05014002.
- de Almeida, E., & Hofland, B. (2020). Validation of pressure-impulse theory for standing wave impact loading on vertical hydraulic structures with short overhangs. *Coastal Engineering*, 159, 103702.
- Didenkulova, I. and Pelinovsky, E. (2011) “Runup of tsunami waves in U-shaped bays”, *Pure and Applied Geophysics*, 168, 123901249.
- Esteban, M., Onuki, M., Ikeda, I. and Akiyama, T. (2015) “Reconstruction Following the 2011 Tohoku Earthquake Tsunami: Case Study of Otsuchi Town in Iwate Prefecture, Japan” in *Handbook of Coastal Disaster Mitigation for Engineers and Planners*. Esteban, M., Takagi, H. and Shibayama, T. (eds.). Butterworth-Heinemann (Elsevier), Oxford, UK
- FEMA. (2012). *Guidelines for Design of Structures for Vertical Evacuation from Tsunamis*. California.
- Glasbergen, T. (2017) “Characteristics of incoming tsunamis for the design of coastal structures”, Master Thesis, Delft: Delft University of Technology.
- Goda, Y., Haranaka, S., Kitahata, M (1966). Study on impulsive breaking wave forces on piles. Report of the Port and Harbour Technical Research Institute, 5, 1–30.
- Google. (2019, June 19). Japan. Retrieved from Google Maps: <https://www.google.com/maps/place/Japan/@39.2940583,141.6539264,8.75z/data=!4m5!3m4!1s0x34674e0fd77f192f:0xf54275d47c665244!8m2!3d36.204824!4d138.252924>
- Grilli, S. T., Member ASCE, Svendsen, I. A., Member ASCE and Subramanya, R. (1997) “Breaking criterion and characteristics for solitary waves on slopes”, *Journal of Waterway Port Coastal and Ocean Engineering*, 123 (3), 102-112.
- Grue, J. , Pelinovsky, E. N., Fructus, D., Talipova, T. and Kharif, C. (2008). “Formation of undular bores and solitary waves in the Strait of Malacca caused by the 26 December 2004 Indian Ocean tsunami”. *Journal of Geophysical Research*, 113 (C05008).
- Jayaratne, M. P. R., Premaratne, B., Adewale, A., Mikami, T., Matsuba, S. Shibayama, T., Esteban, M. and Nistor, I. (2016) “Failure Mechanisms and Local Scour at Coastal Structures Induced by Tsunami”, *Coastal Engineering Journal* 58 (04)
- Koch, C., & Chanson, H. (2009). “Turbulence measurements in positive surges and bores”. *Journal of Hydraulic Research*, 47(1), 29-40.
- Larsen, B. and Fuhrman, D.R. (2019) “Full-scale CFD simulation of tsunamis. Part 1: Model validation and run-up”, *Coastal Engineering*, 151, 22-41
- Lipa, B., Barrick, D. and Isaacson, J. (2016) “Coastal Tsunami Warning with Deployed HF Radar Systems”, In Mokhtari, M., *Tsunami* (pp. 73-111). Rijeka: InTechOpen.
- Liu, P. L.-F. (2009). “Tsunami”. In J. H. Steele, *Encyclopedia of Ocean Sciences* (pp. 127-140). Massachusetts.
- Madsen, P. A., Fuhrman, D. R., & Schäffer, H. A. (2008). “On the solitary wave paradigm for tsunamis”. *Journal of Geophysical Research: Oceans*, 113(C12).
- Madsen, P.A. and Fuhrman, D.R. (2008) “Runup of tsunamis and long waves in terms of surf-similarity”, *Coastal Engineering Journal*, 55 (3), 209–224
- Mori, N., Takahashi T. and The 2011 Tohoku Earthquake Tsunami Joint Survey Group (2012) “Nationwide survey of the 2011 Tohoku earthquake tsunami”, *Coastal Engineering Journal*, 54 (1), 1-27
- Mikami, T., Shibayama, T., Esteban, M. and Matsumaru, R., (2012) “Field Survey of the 2011 Tohoku Earthquake and Tsunami in Miyagi and Fukushima Prefectures”, *Coastal Engineering Journal (CEJ)*, 54 (1), 1-26

- Navionics. (n.d.). Chart Viewer. Retrieved from Navionics:
<https://webapp.navionics.com/?lang=en#boating@5&key=oaioFuwg%7BY>
- Peregrine, DH, 1966. Calculations of the development of an undular bore. *Journal of Fluid Mechanics*, 25(2), 321-330.
- Rijnsdorp, D.P. P.B. Smit and M. Zijlema, 2014. [Non-hydrostatic modelling of infragravity waves under laboratory conditions](#). *Coastal Engineering*, 85, 30-42.
- Rijnsdorp, D.P., G.Ruessink and M. Zijlema, 2015. [Infragravity-wave dynamics in a barred coastal region, a numerical study](#). *Journal of Geophysics Research Oceans*, 120, 4068-4089.
- Roubos, J. (2019) Prediction of the characteristics of a tsunami wave near the Tohoku coastline – Numerical SWASH modelling. MSc thesis. Delft University of Technology. doi: <http://resolver.tudelft.nl/uuid:421cd6b8-fd31-424a-aa9b-529dc17018eb>
- Sainflou, M. (1928). *Essai sur les diques maritimes verticales*. Technical report, Paris.
- Shibayama, T., Esteban, M., Nistor, I., Takagi, H., Danh Thao, N., Matsumaru, R., Mikami, T., Aranguiz, R., Jayaratne, R. and Ohira, K. (2013) “Classification of Tsunami and Evacuation Areas”, *Journal of Natural Hazards*, 67 (2), 365-386
- Shimonzono, T., Sato, S., Okayasu, A., Tajima, Y., Fritz, H. M., Liu, H., and Takagawa, T. (2012) “Propagation and inundation characteristics of the 2011 Tohoku Tsunami on the central Sanriku coast”, *Coastal Engineering Journal*, 54 (1), 1250004-1-1250004-17
- Shimozono, T. 2016 Long wave propagation and run-up in converging bays. *Journal of Fluid Mechanics* 798, 457-484.
- Shuto, N., 1985. Nihonkai-Chubu earthquake tsunami on the north Akita coast. *Coastal Engineering Japan* 28, 255–264.
- Smit, P., Zijlema, M. and Stelling, G. (2013) “Depth-induced wave breaking in a non-hydrostatic, near-shore wave model”, *Coastal Engineering*, 76, 1-16
- Sriram, V., Didenkulova, I., Sergeeva, A., Schimmels, S., 2016. Tsunami evolution and run-up in a large scale experimental facility. *Coastal Engineering* 111, 1–12.
- St-Germain, P., Nistor, I., & Townsend, R. (2012). “Numerical modeling of the impact with structures of tsunami bores propagating on dry and wet beds using the SPH method”. *International Journal of Protective Structures*, 3(2), 221-255.
- Tissier, M., Bonneton, P., Marche, F., Chazel, F. and Lannes, D. (2011) “Nearshore Dynamics of Tsunami-like Undular Bores using a Fully Nonlinear Boussinesq Model”, *Journal of Coastal Research*, 64, 1-6
- Topics, T. (2016, November 25) “Kuji Tsunami Compilation - Japan 2011” [Video File], Retrieved from <https://www.youtube.com/watch?v=ob28xxKT6uE&t=433s>
- Topics, T. (2017, May 9) “Giant Tsunami in Miyako - Final Documentary - Japan 2011” [Video File], Retrieved from <https://www.youtube.com/watch?v=xt6xUuul1s&t=578s>
- Topics, T. (2018, March 6) “Sendai Tsunami Final Edition - Japan 2011 seventh Anniversary” [Video File], Retrieved from <https://www.youtube.com/watch?v=spmTTNInXx8&t=342s>
- Tsuji, Y, Yanuma T, Murata I, Fujiwara C, 1991. Tsunami ascending in rivers as an undular bore. *Natural Hazards*, 4, 257-266.
- Wei, Y., Chamberlin, C., Titov, V. V., Tang, L., and Bernard, E. N. (2012) “Modeling of the 2011 Japan Tsunami: Lessons for Near-Field Forecast”, *Pure and Applied Geophysics*, 170 (6-8), 1309-1331
- Yeh, H. (2006). “Maximum fluid forces in the tsunami runup zone”. *Journal of waterway, port, coastal, and ocean engineering*, 132(6), 496-500.
- Zijlema, M. and Stelling, G.S., 2008. Efficient computation of surf zone waves using the nonlinear shallow water equations with non-hydrostatic pressure. *Coastal Engineering*, 55, 780-790.
- Zijlema, M., Stelling, G. S. and Smit, P. (2011) “SWASH: an operational public domain code for simulating wave fields and rapidly varied flows in coastal waters”, *Coastal Engineering*, 58 (10), 992-1012